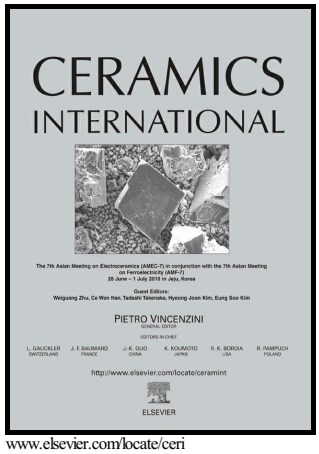


www.elsevier.com/locate/ceri

# Insight into the $BiFeO_3$flash sintering process by *in-situ* energy dispersive X-ray diffraction (ED-XRD)

Luis A. Perez-Maqueda, Eva Gil-Gonzalez, Mary Anne Wassel, Shikhar K. JHA, Antonio Perejon, Harry Charalambous, John Okasinski, Pedro E. Sanchez-Jimenez, Thomas Tsakalakos

PII: S0272-8842(18)32035-2
DOI: https://doi.org/10.1016/j.ceramint.2018.07.293
Reference: CERI19015

To appear in: *Ceramics International*

Cite this article as: Luis A. Perez-Maqueda, Eva Gil-Gonzalez, Mary Anne Wassel, Shikhar K. JHA, Antonio Perejon, Harry Charalambous, John Okasinski, Pedro E. Sanchez-Jimenez and Thomas Tsakalakos, Insight into the $BiFeO_3$flash sintering process by *in-situ* energy dispersive X-ray diffraction (ED-XRD), *Ceramics International,* https://doi.org/10.1016/j.ceramint.2018.07.293

# Insight into the $BiFeO_3$flash sintering process by *in-situ* energy dispersive X-ray diffraction (ED-XRD)

Luis A. Perez-Maqueda[1,2*] Eva Gil-Gonzalez[1], Mary Anne Wassel[2], Shikhar K. JHA[2], Antonio Perejon[1,3], Harry Charalambous[2], John Okasinski[4], Pedro E. Sanchez-Jimenez[1], Thomas Tsakalakos[2]

[1]Instituto de Ciencia de Materiales de Sevilla, (C.S.I.C. - Univ. Sevilla), Americo Vespucio 49, 41092 Sevilla, Spain
[2]Department of Materials Science and Engineering, Rutgers University, 607 Taylor Road, Piscataway, New Jersey 08854, USA
[3]Departamento de Química Inorgánica, Facultad de Química, Universidad de Sevilla, Sevilla 41071, Spain
[4]X-ray Science Division, Advanced Photon Source, Argonne National Laboratory, 9700 South Cass Avenue, Argonne, Illinois 60439, USA

[*]Corresponding author: Tel.: +(34)954489501; fax: [+34] 954460165, maqueda@cica.es

**Abstract** The sintering mechanism of $BiFeO_3$ has been investigated *in-situ* by energy dispersive X-ray diffraction (ED-XRD) using high-energy white collimated X-ray beam from Advanced Photon Source (Argonne National Laboratories). Such radiation is very penetrating thereby allowing measurements of the sample even when placed inside the flash sintering set up. Additionally, the fast ED-XRD measurements permit monitoring the flash sintering process by providing information about phase composition and sample temperature in real time. Moreover, profile scans, obtained by moving the stage vertically while recording the ED-XRD spectra, permits investigating the homogeneity of the flash for the entire length of the sample. All experiments have been complemented by *ex-situ* studies. It has been concluded that flash sintering of $BiFeO_3$ is a homogeneous process without any directionality effects. Furthermore, flash sintering takes place at quite low temperatures (below the Tc ≈ 830$^o$C), which may be related to the high quality of the samples, as pure ceramics without evidence of secondary phases with an homogenous nanostructured grain size distribution and highly insulating are obtained by this technique. Moreover, it is also evidenced that the rapid heating of the sample does not seem to justify, at least by itself, the densification process. Therefore, it appears that the electric current should play a role in the enhanced mobility during sintering process.



## 1. INTRODUCTION

Flash sintering implies applying a small DC current through a ceramic pellet, producing sintering within seconds at furnace temperatures much lower than those required for conventional sintering. Since its discovery in 2010, flash sintering has become a hot topic in ceramic processing with an increasing number of publications (from two in

2010 to more than forty in the last year) [1-4]. It has been successfully applied to a number of ceramic materials, including single and mixed oxides [1, 2, 5-12], carbides [13, 14], and composites [15, 16]. Recently, pure highly-insulating nanostructured $BiFeO_3$ dense pellets have been prepared by flash sintering [17] and directly synthesized by reaction flash-sintering [18]. This is an interesting result considering that $BiFeO_3$ is a metastable phase that easily decomposes into secondary phases, *i.e*. $Bi_{25}FeO_{39}$ and $Bi_2Fe_4O_9$ [19-22], which increase its leakage current [20-23], deteriorating the electrical properties of the material. Moreover, above the Curie Temperature (Tc) transition (about 830$^o$C) the material destabilizes into secondary phases [23, 24]. Unfortunately, sintering usually requires temperatures above 830$^o$C. Thus, most $BiFeO_3$ ceramics have certain amounts of secondary phases [19]. Furthermore, although Spark Plasma Sintering (SPS) has been effectively employed to sinter $BiFeO_3$ ceramics at low temperatures, the $BiFeO_3$ ceramics obtained by the SPS process, exhibit extreme conductivity due to the highly reducing conditions, and an oxidative post-sintering anneal is required [25-27].

Despite growing interest in flash sintering, the densification mechanism is still unknown and controversial [28-33]. However, it is quite clear that a sharp increase in temperatures of several hundreds of degrees, in one or two seconds, is produced by the Joule heating of the sample. The onset temperature of such an event depends on the applied voltage and on the electrical conductivity of the sample. Although ultrafast heating plays a significant role on the sintering process [30], it is unclear whether it is the only effect of flash sintering [29]. In fact, there are issues that do not seem to be justified by Joule heating alone. It appears the electrical current may have some additional effects.

To clarify these open questions, different experimental techniques have been used to perform *in-situ* studies around the effect of the electric field on sintering process. Thus, by *in-situ* high-resolution TEM analysis, it has been observed that electric field changes grain boundary mobility [34] and improves sintering [35]. Besides, optical emission measurements during flash sintering experimentation have shown electroluminescence with fixed wavelength, independent of specimen temperature, corresponding to the band-gap for electron-hole recombination [36]. Moreover, it has been reported that an applied electric field shifts the temperature of phase transitions, such as Curie temperature, Tc [38-41].

One of the most powerful experimental procedures for studying flash sintering under *in-situ* conditions is synchrotron energy dispersive X-ray diffraction (ED-XRD). This method allows determination during the flash event of specimen temperature [36], temperature uniformity [37], lattice expansion [38, 39], and phase composition [40]. Thus, ED-XRD has shown, under simultaneous applied electric and thermal potentials, anomalous lattice expansion in YSZ [38] and $TiB_2$ powder with $TiO_2$ and $TiBO_3$ as secondary phases [41]. Moreover, during the application of electric field during flash sintering of 3YSZ, a new crystallographic phase which disappears when the field is shut off, was observed [40].

The aim of the present article is to utilize the unique capabilities of the *in-situ* synchrotron ED-XRD to provide an insight of the flash sintering mechanism of $BiFeO_3$ that yields pure and highly insulating materials unlike other sintering procedures. Furthermore, this study aims to explore the role of the electric potential used during the flash-sintering

process on the reaction kinetics, beyond the Joule heating effect. Understanding the sintering mechanism of a metastable compound such as $BiFeO_3$ offers new opportunities for applying flash sintering for the densification of other relevant metastable compounds.

## 2. EXPERIMENTAL

Mechanosynthesised $BiFeO_3$ powders were prepared from stoichiometric amounts of the starting oxides, $Bi_2O_3$ (Sigma-Aldrich 223891-500G, 10 µm, 99.9% purity) and $Fe_2O_3$ (Sigma-Aldrich 310050-500G, <5 µm, ≥99% purity), which were milled for 8 hours in a high energy planetary ball mill (Fritsch Pulverisette 7, Fritsch GmbH, Idar-Oberstein, Germany) under 7 bar of oxygen pressure [42]. For the preparation of green pellets for flash sintering experiments, the mechanosynthesised $BiFeO_3$ powders were uniaxially pressed into either cylindrical (¼" diameter, 5 mm thickness) and dog bone shaped (1 mm thickness) pellets.

For *in-situ* energy dispersive X-ray diffraction (ED-XRD), the green cylindrical pellets were placed on a special hot stage, which consists of a spring loaded ceramic specimen holder that is resistively heated. The hot stage was mounted on a positioning stage so that the sample could be stationary for exposure to an ultrahigh energy polychromatic radiation of photons of 200 keV at a fixed Bragg angle. A detailed description of the experimental set up and the technique has been previously described by Akdoğan *et al.* and Özdemir *et al.* [38, 41]. The experiments were carried out in the National Synchrotron Light Source (NSLS) of Argonne National Laboratory (ANL). For the study of densification during conventional heating, a sample pellet was heated at $10^oC\ min^{-1}$ while the

diffraction patterns were collected every 1 second. Flash sintering experiments were performed under isothermal conditions at 350ºC, while a DC potential of 100 V $cm^{-1}$ was applied between two wires attached to opposite ends of the $BiFeO_3$ pellets. Platinum paste was used to increase the electrical contact between the electrodes and the specimen. A typical flash sintering experiment consists of three well-defined stages. Firstly, a small incubation stage (stage I) is followed by a non-linear rise of the specimen conductivity up to the predefined limit, which corresponds to the flash event (stage II). At this point, the power supply is switched from voltage to current controlled mode signaling the beginning of stage III, which is maintained for 75 seconds approximately. As in the conventional heating experiment, *in-situ* ED-XRD data were collected every 1 second.

*Ex-situ* flash sintering experiments were performed using dog bone pellets and an experimental set up similar to that originally proposed by Cologna et al [1].

The density of the samples was measured by the Archimedes' method using distilled water at room temperature as the immersion liquid.

Laboratory X-ray diffraction (XRD) patterns were collected in a Miniflex diffractometer (Rigaku, Japan) working at 45 kV and 40 mA using CuKα radiation. The data were acquired from 15º to 60º using a step size of 0.02º and a scan speed of 0.24 seconds per step.

The microstructure of the samples was studied by scanning electron microscopy (SEM) employing a Hitachi S-4800 SEM-FEG using a field-emission gun operated at 2 kV. In order to reveal the grain structure, the sintered pellets were prepared for SEM by polishing the samples and using a thermal etching for 30 min at 90% of temperature

reached during the sintering experiment. Due to the insulating nature of the samples, the samples were Au sputter-coated using an Emithech K550 Sputter (Telstar, Spain).

Dilatometric studies were performed in cylindrical pellets in air at a heating rate of $10^{o}C\ min^{-1}$ using a TMA PT100 (Linseis, Germany).

Relative permittivity and tan δ measurements as a function of temperature were carried out using a 4263B LCR meter (Agilent Technologies, California, USA) at a fixed frequency of 100 kHz. Opposite pellet faces were previously Au sputter-coated using the Emitech K550 Sputter (Telstar, Spain) analogous to the samples prepared for SEM.

**3. RESULTS**

The governing equations for ED-XRD results from the combination of the Bragg's Law and Planck's equation to relate the scattered energy of the (*hkl*) reflections with the interplanar distance $d_{hkl}$ (in KeV and Å for Eq. 1, respectively):

$$E_{hkl} = \frac{6.1992}{d_{hkl} \sin\theta} \qquad (1)$$

Figure 1a includes a contour plot of diffraction peak intensities as a function of temperature for the conventional sintering experiment. Values of *d*-spacing for (104) and (110) reflections (calculated from equation 1) as a function of the temperature are depicted in Fig. 1b. These figures show the crystal lattice thermal expansion in the temperature range up to about $830^{o}C$ where there is a change in the pattern that corresponds to the α–β or Curie (Tc) transition for $BiFeO_3$ (from rhombohedral *R3c* to orthorhombic *Pnma*). Fig. 1c includes the evolution of the volumetric thermal expansion

coefficient (β) as a function of temperature in the range from 500ºC to 825ºC, which has been calculated from the cell volume expansion that the sample undergoes in that temperature range (see Fig. S1 of the supporting information). As expected, it is observed an increase of the volumetric thermal expansion coefficient with temperature that can be approximated to the following parabolic function:

$$\beta = -9.416 \cdot 10^{-8} T^2 + 1.699 \cdot 10^{-4} T - 0.06062 \qquad (2)$$

The dilatometric curve in Fig. 1d has been corrected considering the thermal expansion coefficients (eq. 2) determined from diffraction measurements. This figure (Fig. 1d) shows sample densification in the range from 425ºC up to about 870ºC, that is accompanied by the reversible volume decrease due to the Curie transition. The overlap of the Curie transition with the densification of the material, has been postulated as one of the reasons for the formation of secondary phases during sintering as the material is very unstable above Curie transition [23].

Figure 2 shows a flash sintering experiment at 350ºC furnace temperature at a constant electric field of 100 V $cm^{-1}$ and a current limit of 2.5 A $cm^{-2}$. This figure includes the evolution of electric field (Fig. 2a), current intensity (Fig. 2b), and power density dissipated (Fig. 2c) as a function of time. The experiment has three stages that have been marked in the figure. First, a small incubation stage (marked as I in Fig. 2c) is followed by a sharp increase in current intensity up to the predefined limit that corresponds to the flash event (marked as II); Second, the power supply shifts to current-controlled mode and it is maintained for 75 seconds (marked as III) and; Third, the power supply was switched off.

During the flash sintering experiment, the evolution of the sample was monitored by *in-situ* ED-XRD. The contour plot of diffraction peak intensities as a function of temperature with the overlaid fitting is shown in Fig. 3a). Using equation 1, resulting values of *d*-spacing for (104) and (110) reflections as a function of time (Fig. 3b)) demonstrate that once the power supply is turned on, there is a sharp crystal lattice expansion preceded by a small induction period. This lattice expansion is associated to the sharp Joule heating of the specimen produced by the flow of the electric current through the sample. The temperature reached by the pellet was estimated from comparison of the values of the *d*-spacing measured during the flash event, with those determined during conventional sintering. The results are summarized in Fig. 1. The maximum reached values for *d*-spacing during the flash were approximately 2.844 Å and 2.818 Å for (104) and (110) reflections, respectively. These, corresponds to the values at approximately 783$^{o}$C which is considerably lower with respect to 830$^{o}$C at which the Curie transition takes place (Fig. 3b). Moreover, the two diffraction peaks corresponding to the low temperature rhombohedral phase were observed during the entire flash sintering experiment without any evidence of a change to the high temperature orthorhombic *Pnma* phase that would imply having passed through the Tc.

The analysed SEM picture depicted in Fig. 4a shows that the microstructure of the material flash sintered, under the conditions given in Fig. 2, corresponds to a well-sintered ceramic with low porosity and nanometric grains. The relative density of the pellet, measured by the Archimede's method, is 90%. Moreover, it can be inferred from Fig. 4b that the experimental XRD pattern of $BiFeO_3$ fits very well the calculated pattern, using a

R3c space group, with good confident factor (see Table S1 for further information). This is an indication that the sample is pure with no evidence of secondary phases. Figure 5 presents fixed-frequency (100 kHz) plots of relative permittivity $\varepsilon_r'$ (Fig. 5a), and *tan* δ (Fig.5b) from room temperature to 200$^o$C for the flash-sintered sample. The relative permittivity increased in the range ~110-135 with temperature, as expected, for a ferroelectric material below its Tc. Moreover, the values of *tan* δ are small and increase from 180-200$^o$C, which indicates that the sample is a good dielectric in the temperature range studied.

Figure 6 depicts a diagram of the profile scan of an *in-situ* flash-sintering experiment under the conditions described in Fig. 2. For the experiment, the sample stage was moved vertically (upwards and downwards). Since the source and detector were fixed in space, the gauge volume of diffraction moved from top to the bottom of the specimen height (4.2 mm). The spatial resolution of scans was 0.2 mm and the acquisition time was 10 seconds. The entire experiment was performed during Stage III of flash sintering. This stage is the final part of the process and corresponds to the current intensity-control period, just after reaching the current limit. Such an experiment was performed at this stage because it could be maintained during the time required for the measurements. In the *in-situ* contour plot of the scans (peak intensities) across the flashed pellet, both sample and Pt electrodes on top and bottom could be identified. The diffraction peaks corresponding to the sample were recorded at the same energy values within the entire length of the pellet with no evidence of any anisotropic heating that would result in

differential peak positions within the sample. This suggests that homogeneous flash conditions were achieved during the performed experiment.

## 4. DISCUSSION

Results from the *in-situ* ED-XRD experiments carried out in this work, show that during flash-sintering process of $BiFeO_3$, the material does not undergo the Curie transition and it retains the low-temperature rhombohedral structure. The latter aspect might be key in the high purity of the resulting materials, as it has been previously reported in the literature that the high-temperature orthorhombic phase, readily destabilizes into the formation of secondary phases [23]. It is quite interesting that the material sinters at relatively low temperatures producing high-density nanostructured pellets. It has been recently postulated by Ji et al [30], when studying flash sintering of YSZ, that the fast densification could be at least partially attributed to the rapid heating of the specimen during the flash sintering experiment. To further investigate this effect for $BiFeO_3$, a very small cylindrical sample (6 mm in diameter by 0.9 mm thickness), to minimize heat transfer phenomena, was introduced in a furnace previously heated at 820$^{o}$C, which is above the temperature reached during the flash sintering experiment and just below the $T_c$ to avoid sample decomposition. Then, it was maintained into the furnace for 75 seconds and, finally, quenched at room temperature. Sample temperature was monitored with a thermocouple placed next to it. Thus, once the sample was introduced in the furnace, it was observed that it reached immediately the desired temperature. The characteristic SEM micrograph of the resulting material (Fig. 7) shows that the

microstructure of the pellet corresponds to a poorly sintered material with very high porosity and a relative density as measured by the Archimedes method, of less than 80%. Moreover, unlike the flash-sintered sample which is pure (Fig. 4a), the XRD pattern of this pellet (Fig. S2) shows that it contains minor amounts of $Bi_{25}FeO_{39}$. Thus, besides the obvious effect on the purity, rapid heating cannot explain alone the high density of the $BiFeO_3$ flash-sintered sample prepared in this work. Therefore, current should play some additional role to the Joule heating. Our results are in agreement with other studies that have proven an increase in diffusion and mass transport, due to the electric current [43-49]. On the present case, it could justify the enhanced densification for $BiFeO_3$ in the presence of the electric field.

Moreover, the effect of directionality of the electric field on the microstructure of the samples is another issue related to DC flash sintered ceramics. For example, for ionic conductors such as YSZ [50, 51] and $MgAl_2O_4$ [52], a grain size gradient through the specimen has been observed, from increase in the average grain size towards the cathode. This behavior has been explained by the need of a reversible electrochemical reaction for the ionic conduction mechanism [53]. Moreover, for semiconductors such as ZnO, it has been reported that flash sintered samples show an enhanced grain growth at the anode for high current intensities [54]. The origin of such behavior is unknown and harder to explain than for ionic conductors but some theories, such as a Peltier effect with cold and hot sample ends, electrochemical effects and flow of ionic current have been postulated [28, 54]. For flash sintering of $BiFeO_3$, the profile scan presented in Fig. 6 shows a homogeneous flash with observed peak positons at the same values of energy within the

full sample length suggesting a homogeneous temperature in the entire pellet during the flash event. These observations agree with reports for other materials that show only small temperature gradients within the sample during the flash [37].

In order to further investigate a possible directionality, an independent flash sintering experiment was performed in the laboratory (Fig. 8). In this experiment, a dog bone shaped sample was flash sintered and analyzed in detail at different positions corresponding to the central area and to spots located close to the positive and negative electrodes (highlighted in Fig. 8a). No significant differences were observed in terms of density (above 90%) or microstructure within the different studied regions. Identical nanometric grains and no porosity are observed in the SEM analysis of all three studied areas (Fig. 8b). Moreover, X-ray diffraction patterns, of the different sections after the flash are almost identical with slight changes in the relative intensity of the peaks, which may be attributed to preferred orientations effects. This fact confirms the pure perovskite phase for all the studied regions (Fig. 8c). These results are in contrast with previously reported for $BaTiO_3$ samples in which secondary phases are found to form from the flash sintering process [55]. Nevertheless, previous observations also suggest that in order to avoid secondary phases during flash sintering of $BaTiO_3$, the electric and current should be maintained within an optimum processing range (133 V $cm^{-1}$ and 500 mA, respectively). For $BiFeO_3$, it has been previously reported that the electric field and current should be maintained within an optimum processing range to obtain high purity materials, otherwise, secondary phases are detected [17, 18].

Finally, it is worth noting that the sample obtained by flash sintering is highly insulating, as it is shown in Fig. 5, where there is no evidence of leakage currents unlike non-stoichiometric materials [56-62]. In addition to this behavior being a clear indication of the high purity of the sample, it also reveals a very low concentration of oxygen vacancies, if present. This latter aspect is in contrast with other reports that have shown electrochemical reduction of the sample during field assisted sintering. For flash sintering and reaction flash-sintering of $BiFeO_3$ relatively mild conditions are required. In contrast, for SPS sintered $BiFeO_3$ pellets, high sample conductivity has been reported and can be attributed to the reduction of the sample during the sintering process as a consequence of the high current intensities and high vacuum used in the experiments [25, 27].

## 5. CONCLUSIONS

A High-quality $BiFeO_3$ ceramic in terms of purity, with an homogeneous nanostructured grain size distribution and highly insulating at room temperature has been prepared by flash sintering. It has been proved that energy dispersive X-ray diffraction (ED-XRD) is a very useful technique for studying the flash sintering process of $BiFeO_3$ under *in-situ* conditions. The high purity of the resulting material could be explained by considering that the temperature reached by the sample during the flash-sintering process carried out in this work, is well below the $T_C$. Moreover, the high temperature orthorhombic phase, which destabilizes into secondary phases, was not detected. The latter seems to have prevented thermal decomposition. Moreover, the high density nanostructured microstructure could not be fully explained just by the rapid Joule heating

of the sample during the flash process. Thus, it is speculated that current should play some role, facilitating the mobility during the sintering.

Furthermore, in a profile scan obtained by moving the stage vertically it was concluded that the flash is quite homogeneous suggesting a constant temperature throughout the samples. *Ex-situ* studies confirmed the homogeneity in terms of structure and microstructure all over the entire length of the sample (from cathode to anode).

All in all, it is worthy to note that *in-situ* energy dispersive X-ray diffraction (ED-XRD) is proven to be a powerful technique for providing insight into the flash-sintering behavior of a metastable compound such as $BiFeO_3$. This methodology can be extrapolated to the study of other relevant metastable compounds.



**ACKNOWLEDGEMENT**

The authors wish to express their gratitude for the financial support provided by the Office of Naval Research (ONR) under Contract No. N00014-10-1-042 and Contract No. N00014-17-1-2087 Sub-Award No. 4104-78982 from Purdue. The authors wish to thank Dr. Antti Makinen of the ONR for his support of this project valuable technical feedback. This research used resources of the Advanced Photon Source, a U.S. Department of Energy Office of Science User Facility operated for the DOE Office of Science by Argonne National Laboratory under Contract No. DE-AC02-06CH11357

Financial support from Projects CTQ2014-52763-C2-1-R, CTQ2017-83602-C2 (MINECO-FEDER) and TEP-7858 (Junta Andalucía-FEDER) is acknowledged. AP thanks VPPI-US for his contract.

## REFERENCES


[1] M. Cologna, B. Rashkova, R. Raj, Flash Sintering of Nanograin Zirconia in <5 s at 850°C, Journal of the American Ceramic Society, 93 (2010) 3556-3559.

[2] A.L.G. Prette, M. Cologna, V. Sglavo, R. Raj, Flash-sintering of Co2MnO4 spinet for solid oxide fuel cell applications, Journal of Power Sources, 196 (2011) 2061-2065.

[3] M. Cologna, J.S.C. Francis, R. Raj, Field assisted and flash sintering of alumina and its relationship to conductivity and MgO-doping, Journal of the European Ceramic Society, 31 (2011) 2827-2837.

[4] M. Cologna, A.L.G. Prette, R. Raj, Flash-Sintering of Cubic Yttria-Stabilized Zirconia at 750 degrees C for Possible Use in SOFC Manufacturing, Journal of the American Ceramic Society, 94 (2011) 316-319.

[5] J.A. Downs, V.M. Sglavo, Electric Field Assisted Sintering of Cubic Zirconia at 390 degrees C, Journal of the American Ceramic Society, 96 (2013) 1342-1344.

[6] A. Gaur, V.M. Sglavo, Flash-sintering of MnCo2O4 and its relation to phase stability, Journal of the European Ceramic Society, 34 (2014) 2391-2400.

[7] A. Karakuscu, M. Cologna, D. Yarotski, J. Won, J.S.C. Francis, R. Raj, B.P. Uberuaga, Defect Structure of Flash-Sintered Strontium Titanate, Journal of the American Ceramic Society, 95 (2012) 2531-2536.

[8] S.K. Jha, R. Raj, The Effect of Electric Field on Sintering and Electrical Conductivity of Titania, Journal of the American Ceramic Society, 97 (2014) 527-534.

[9] I. Bajpai, Y.-H. Han, J. Yun, J. Francis, S. Kim, R. Raj, Preliminary investigation of hydroxyapatite microstructures prepared by flash sintering, Advances in Applied Ceramics, 115 (2016) 276-281.

[10] J.-C. M'Peko, J.S.C. Francis, R. Raj, Field-assisted sintering of undoped BaTiO3: Microstructure evolution and dielectric permittivity, Journal of the European Ceramic Society, 34 (2014) 3655-3660.

[11] L.M. Jesus, R.S. Silva, R. Raj, J.-C. M'Peko, Electric field-assisted flash sintering of CaCu3Ti4O12: Microstructure characteristics and dielectric properties, Journal of Alloys and Compounds, 682 (2016) 753-758.

[12] Y. Zhang, J. Luo, Promoting the flash sintering of ZnO in reduced atmospheres to achieve nearly full densities at furnace temperatures of <120°C, Scripta Materialia, 106 (2015) 26-29.

[13] E. Zapata-Solvas, S. Bonilla, P.R. Wilshaw, R.I. Todd, Preliminary investigation of flash sintering of SiC, Journal of the European Ceramic Society, 33 (2013) 2811-2816.

[14] V.M. Candelario, R. Moreno, R.I. Todd, A.L. Ortiz, Liquid-phase assisted flash sintering of SiC from powder mixtures prepared by aqueous colloidal processing, Journal of the European Ceramic Society, 37 (2017) 485-498.

[15] A. Gaur, V.M. Sglavo, Flash Sintering of (La, Sr)(Co, Fe)$O_3$-Gd-Doped $CeO_2$ Composite, Journal of the American Ceramic Society, 98 (2015) 1747-1752.

[16] D. Kok, S.K. Jha, R. Raj, M.L. Mecartney, Flash sintering of a three-phase alumina, spinel, and yttria-stabilized zirconia composite, Journal of the American Ceramic Society, DOI: 10.1111/jace.14818.

[17] L.A. Perez-Maqueda, E. Gil-Gonzalez, A. Perejon, J.M. Lebrun, P.E. Sanchez-Jimenez, R. Raj, Flash sintering of highly insulating nanostructured phase-pure BiFeO3, Journal of the American Ceramic Society, (2017).

[18] E. Gil-Gonzalez, A. Perejon, P.E. Sanchez-Jimenez, M.J. Sayagues, R. Raj, L.A. Perez-Maqueda, Phase-pure BiFeO3 produced by reaction flash-sintering of $Bi_2O_3$ and $Fe_2O_3$, Journal of Materials Chemistry A, 6 (2018) 5356-5366.

[19] S.M. Selbach, M.-A. Einarsrud, T. Grande, On the Thermodynamic Stability of $BiFeO_3$, Chemistry of Materials, 21 (2009) 169-173.

[20] T.T. Carvalho, P.B. Tavares, Synthesis and thermodynamic stability of multiferroic $BiFeO_3$, Materials Letters, 62 (2008) 3984-3986.

[21] A. Maître, M. François, J.C. Gachon, Experimental study of the $Bi_2O_3$-$Fe_2O_3$ pseudo-binary system, Journal of Phase Equilibria and Diffusion, 25 (2004) 59-67.

[22] M.S. Bernardo, T. Jardiel, M. Peiteado, A.C. Caballero, M. Villegas, Reaction pathways in the solid state synthesis of multiferroic $BiFeO_3$, Journal of the European Ceramic Society, 31 (2011) 3047-3053.

[23] A. Perejon, P.E. Sanchez-Jimenez, J.M. Criado, L.A. Perez-Maqueda, Thermal Stability of Multiferroic BiFeO3: Kinetic Nature of the beta-gamma Transition and Peritectic Decomposition, Journal of Physical Chemistry C, 118 (2014) 26387-26395.

[24] D.C. Arnold, K.S. Knight, F.D. Morrison, P. Lightfoot, Ferroelectric-Paraelectric Transition in $BiFeO_3$: Crystal Structure of the Orthorhombic beta Phase, Physical Review Letters, 102 (2009).

[25] A. Perejon, N. Maso, A.R. West, P.E. Sanchez-Jimenez, R. Poyato, J.M. Criado, L.A. Perez-Maqueda, Electrical Properties of Stoichiometric $BiFeO_3$ Prepared by Mechanosynthesis with Either Conventional or Spark Plasma Sintering, Journal of the American Ceramic Society, 96 (2013) 1220-1227.

[26] Z.-H. Dai, Y. Akishige, BiFeO3 ceramics synthesized by spark plasma sintering, Ceramics International, 38 (2012) S403-S406.

[27] T. Wang, S.H. Song, M. Wang, J.Q. Li, M. Ravi, Effect of annealing atmosphere on the structural and electrical properties of BiFeO3 multiferroic ceramics prepared by sol-gel and spark plasma sintering techniques, Ceramics International, 42 (2016) 7328-7335.

[28] M. Yu, S. Grasso, R. McKinnon, T. Saunders, M.J. Reece, Review of flash sintering: materials, mechanisms and modelling, Advances in Applied Ceramics, 116 (2017) 24-60.

[29] R. Raj, Joule heating during flash-sintering, Journal of the European Ceramic Society, 32 (2012) 2293-2301.

[30] W. Ji, B. Parker, S. Falco, J.Y. Zhang, Z.Y. Fu, R.I. Todd, Ultra-fast firing: Effect of heating rate on sintering of 3YSZ, with and without an electric field, Journal of the European Ceramic Society, 37 (2017) 2547-2551.

[31] K.S. Naik, V.M. Sglavo, R. Raj, Flash sintering as a nucleation phenomenon and a model thereof, Journal of the European Ceramic Society, 34 (2014) 4063-4067.

[32] J.S.C. Francis, M. Cologna, R. Raj, Particle size effects in flash sintering, Journal of the European Ceramic Society, 32 (2012) 3129-3136.

[33] J.C.S. Francis, R. Rishi, Influence of the Field and the Current Limit on Flash Sintering at Isothermal Furnace Temperatures, Journal of the American Ceramic Society, 96 (2013) 2754-2758.

[34] J.F. Rufner, D. Kaseman, R.H.R. Castro, K. van Benthem, G. Rohrer, DC Electric Field-Enhanced Grain-Boundary Mobility in Magnesium Aluminate During Annealing, Journal of the American Ceramic Society, 99 (2016) 1951-1959.

[35] H. Majidi, K. van Benthem, Consolidation of Partially Stabilized ZrO_{2} in the Presence of a Noncontacting Electric Field, Phys Rev Lett, 114 (2015) 195503.

[36] K. Terauds, J.-M. Lebrun, H.-H. Lee, T.-Y. Jeon, S.-H. Lee, J.H. Je, R. Raj, Electroluminescence and the measurement of temperature during Stage III of flash sintering experiments, Journal of the European Ceramic Society, 35 (2015) 3195-3199.

[37] J.M. Lebrun, S.K. Jha, S.J. McCormack, W.M. Kriven, R. Raj, H. Chan, Broadening of Diffraction Peak Widths and Temperature Nonuniformity During Flash Experiments, Journal of the American Ceramic Society, 99 (2016) 3429-3434.

[38] E.K. Akdoğan, İ. Şavklıyıldız, H. Biçer, W. Paxton, F. Toksoy, Z. Zhong, T. Tsakalakos, Anomalous lattice expansion in yttria stabilized zirconia under simultaneous applied electric and thermal fields: A time-resolved in situ energy dispersive x-ray diffractometry study with an ultrahigh energy synchrotron probe, Journal of Applied Physics, 113 (2013) 233503.

[39] J.M. Lebrun, C.S. Hellberg, S.K. Jha, W.M. Kriven, A. Steveson, K.C. Seymour, N. Bernstein, S.C. Erwin, R. Raj, In-situ measurements of lattice expansion related to defect generation during flash sintering, Journal of the American Ceramic Society, 100 (2017) 4965-4970.

[40] J.M. Lebrun, T.G. Morrissey, J.S.C. Francis, K.C. Seymour, W.M. Kriven, R. Raj, Emergence and Extinction of a New Phase during On-Off Experiments Related to Flash Sintering of 3YSZ, Journal of the American Ceramic Society, 98 (2015) 1493-1497.

[41] T.E. Özdemir, E.K. Akdoğan, İ. Şavklıyıldız, H. Biçer, M. Örnek, Z. Zhong, T. Tsakalakos, Electric field effect on chemical and phase equilibria in nano-TiB2–TiO2–TiBO3 system at <650 °C: an in situ time-resolved energy dispersive x-ray diffraction study with an ultrahigh energy synchrotron probe, Journal of Materials Research, 32 (2016) 482-494.

[42] A. Perejon, N. Murafa, P.E. Sanchez-Jimenez, J.M. Criado, J. Subrt, M.J. Dianez, L.A. Perez-Maqueda, Direct mechanosynthesis of pure $BiFeO_3$ perovskite nanoparticles: reaction mechanism, Journal of Materials Chemistry C, 1 (2013) 3551-3562.

[43] K.J.D. Mackenzie, R.K. Banerjee, M.R. Kasaai, Effect of electric-field on solid-state reactions between oxides.1. Reaction between calcium and aluminum-oxides Journal of Materials Science, 14 (1979) 333-338.

[44] C. Korte, N.D. Zakharov, D. Hesse, Electric field driven solid state reactions—microscopic investigation of moving phase boundaries in the system MgO/MgIn2O4/In2O3, Phys. Chem. Chem. Phys., 5 (2003) 5530-5535.

[45] T. Kondo, M. Yasuhara, T. Kuramoto, Y. Kodera, M. Ohyanagi, Z.A. Munir, Effect of pulsed DC current on atomic diffusion of Nb-C diffusion couple, Journal of Materials Science, 43 (2008) 6400-6405.

[46] C.T. Li, Y.H. Chen, C.N. Liao, Electrically motivated atomic migration and defect formation in Bi0.5Sb1.5Te3 compounds, Materials Chemistry and Physics, 204 (2018) 373-377.

[47] T.B. Holland, U. Anselmi-Tamburini, D.V. Quach, T.B. Tran, A.K. Mukherjee, Local field strengths during early stage field assisted sintering (FAST) of dielectric materials, Journal of the European Ceramic Society, 32 (2012) 3659-3666.

[48] K. Li, X. Wang, Effect of pulsed current on the microstructure evolution of Cu–Sn intermetallic compounds, Materials Science and Technology (United Kingdom), 33 (2017) 2097-2101.

[49] J.T. Cahill, V.R. Vasquez, S.T. Misture, D. Edwards, O.A. Graeve, Effect of Current on Diffusivity in Metal Hexaborides: A Spark Plasma Sintering Study, ACS Applied Materials and Interfaces, 9 (2017) 37357-37363.

[50] S.-W. Kim, S.G. Kim, J.-I. Jung, S.-J.L. Kang, I.W. Chen, J. Roedel, Enhanced Grain Boundary Mobility in Yttria-Stabilized Cubic Zirconia under an Electric Current, Journal of the American Ceramic Society, 94 (2011) 4231-4238.

[51] W. Qin, H. Majidi, J. Yun, K. van Benthem, L. Gauckler, Electrode Effects on Microstructure Formation During FLASH Sintering of Yttrium-Stabilized Zirconia, Journal of the American Ceramic Society, 99 (2016) 2253-2259.

[52] H. Yoshida, P. Biswas, R. Johnson, M.K. Mohan, Flash-sintering of magnesium aluminate spinel (MgAl2O4) ceramics, Journal of the American Ceramic Society, 100 (2017) 554-562.

[53] L.B. Caliman, R. Bouchet, D. Gouvea, P. Soudant, M.C. Steil, Flash sintering of ionic conductors: The need of a reversible electrochemical reaction, Journal of the European Ceramic Society, 36 (2016) 1253-1260.

[54] Y. Zhang, J.-I. Jung, J. Luo, Thermal runaway, flash sintering and asymmetrical microstructural development of ZnO and ZnO–Bi2O3 under direct currents, Acta Materialia, 94 (2015) 87-100.

[55] H. Yoshida, A. Uehashi, T. Tokunaga, K. Sasaki, T. Yamamoto, Formation of grain boundary second phase in $BaTiO_3$ polycrystal under a high DC electric field at elevated temperatures, Journal of the Ceramic Society of Japan, 124 (2016) 388-392.

[56] M. Muneeswaran, R. Dhanalakshmi, N.V. Giridharan, Structural, vibrational, electrical and magnetic properties of Bi1−xPrxFeO3, Ceramics International, 41 (2015) 8511-8519.

[57] Y.P. Wang, L. Zhou, M.F. Zhang, X.Y. Chen, J.M. Liu, Z.G. Liu, Room-temperature saturated ferroelectric polarization in BiFeO3 ceramics synthesized by rapid liquid phase sintering, Applied Physics Letters, 84 (2004) 1731-1733.

[58] S.R. Das, R.N.P. Choudhary, P. Bhattacharya, R.S. Katiyar, P. Dutta, A. Manivannan, M.S. Seehra, Structural and multiferroic properties of La-modified BiFeO[sub 3] ceramics, Journal of Applied Physics, 101 (2007) 034104.

[59] G.L. Yuan, S.W. Or, Y.P. Wang, Z.G. Liu, J.M. Liu, Preparation and multi-properties of insulated single-phase BiFeO 3 ceramics, Solid State Communications, 138 (2006) 76-81.

[60] G.W. Pabst, L.W. Martin, Y.H. Chu, R. Ramesh, Leakage mechanisms in $BiFeO_3$ thin films, Applied Physics Letters, 90 (2007).

[61] X. Qi, J. Dho, R. Tomov, M.G. Blamire, J.L. MacManus-Driscoll, Greatly reduced leakage current and conduction mechanism in aliovalent-ion-doped $BiFeO_3$, Applied Physics Letters, 86 (2005) 1-3.

[62] H. Yang, M. Jain, N.A. Suvorova, H. Zhou, H.M. Luo, D.M. Feldmann, P.C. Dowden, R.F. Depaula, S.R. Foltyn, Q.X. Jia, Temperature-dependent leakage mechanisms of $Pt/BiFeO_3/SrRuO_3$ thin film capacitors, Applied Physics Letters, 91 (2007).

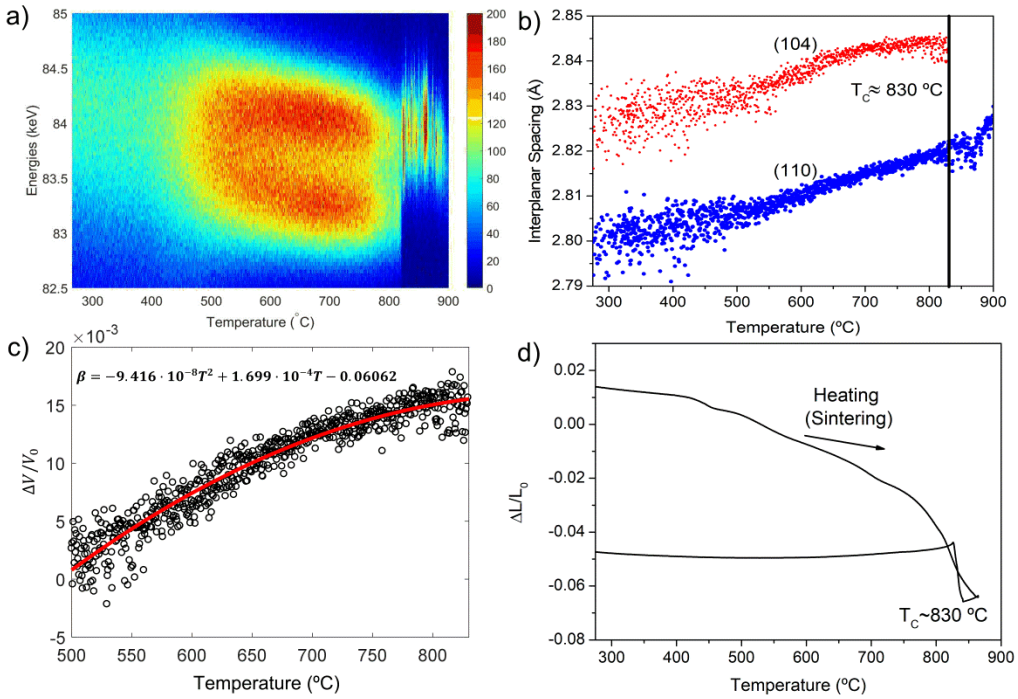


Figure 1. a) Contour plot of diffraction peak intensities as a function of temperature for the conventional sintering experiment of $BiFeO_3$. b) Corresponding *d*-spacing values for (104) and (110) reflections. c) Evolution of the volumetric thermal expansion coefficient as a function of temperature. d) Corrected dilatometric curve as a function of temperature for the conventional sintering experiment of $BiFeO_3$ along with the linear thermal expansion coefficient calculated during cooling.

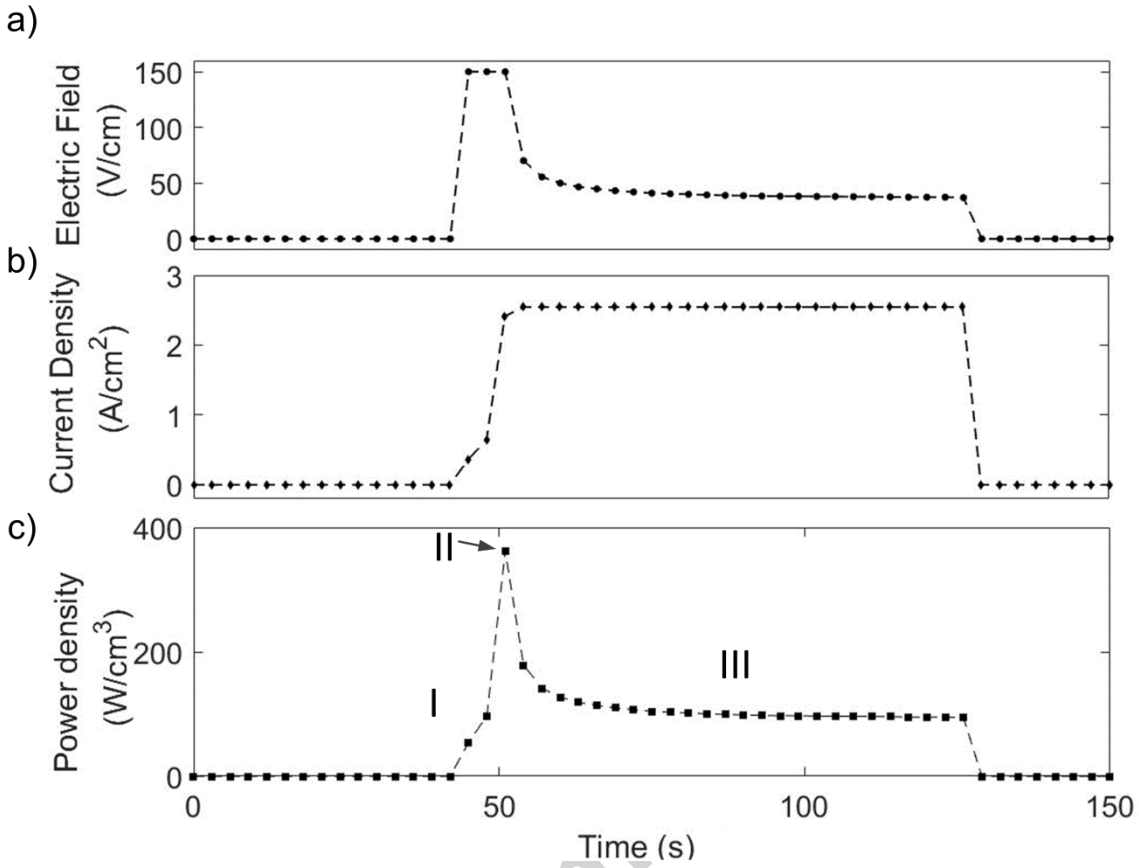


Figure 2. Evolution of a) the electric field, b) current density and b) power density dissipated as a function of time for a flash sintering experiment of a $BiFeO_3$ pellet at a furnace temperature of 350ºC. The constant electric field applied was 100 V $cm^{-1}$ and the current limit was set at 2.5 A $cm^{-2}$.

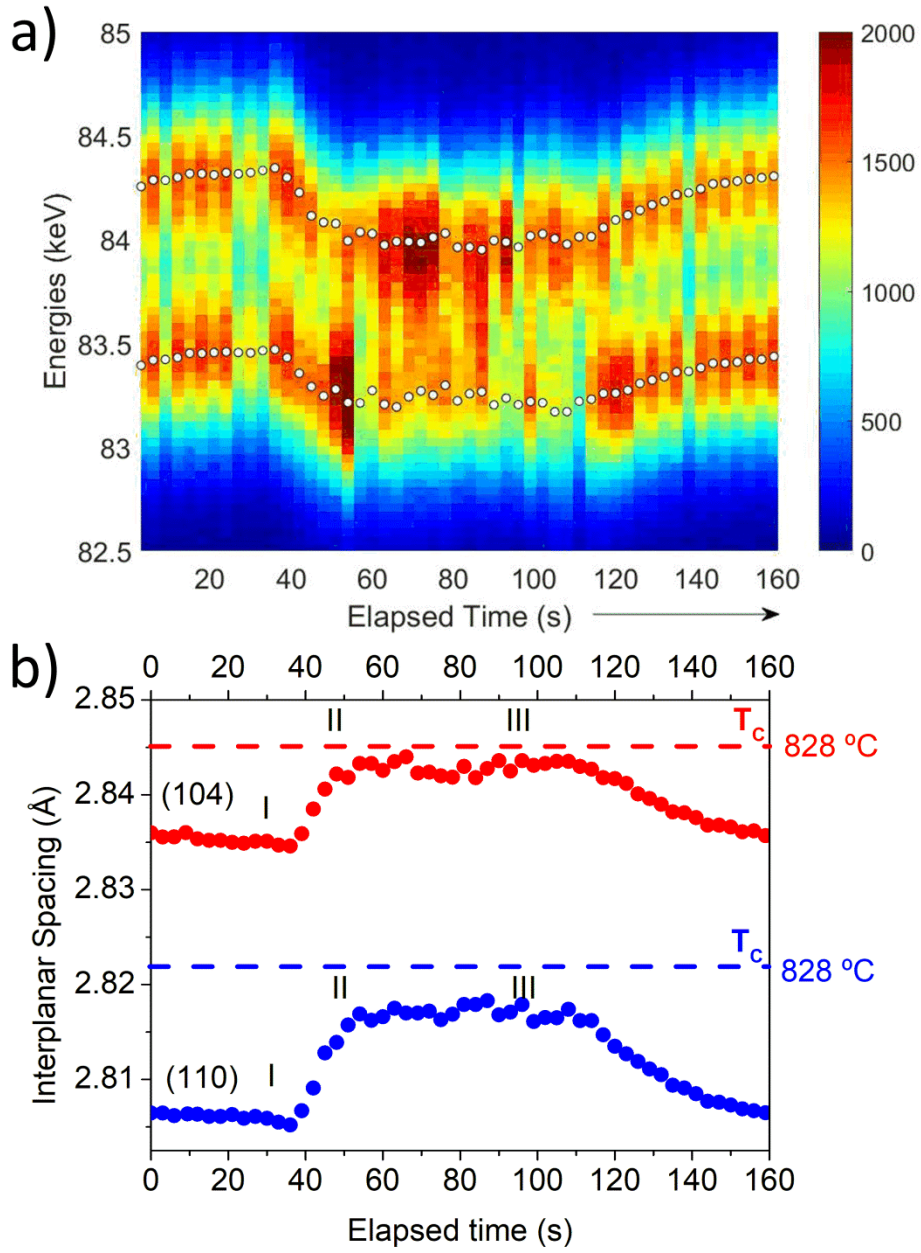


Figure 3. a) Contour plot of diffraction peak intensities and b) Evolution of the interplanar *d*-spacing values for the (104) and (110) diffractions as a function of time during the flash sintering experiment shown in Fig. 2 for a $BiFeO_3$ pellet.

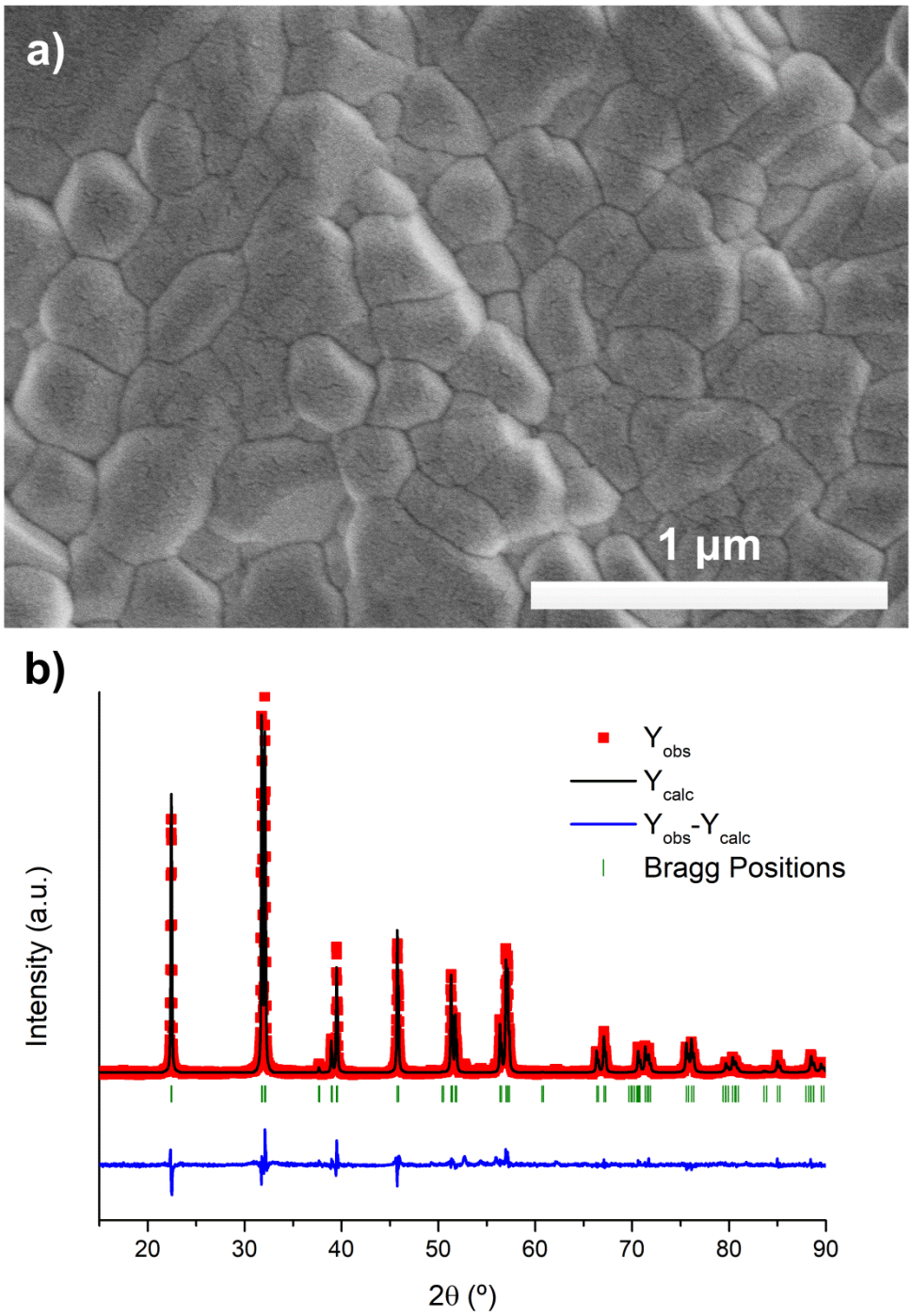


Figure 4. a) SEM micrograph and b) XRD pattern of the $BiFeO_3$ pellet prepared by mechanosynthesis and flash sintered under the conditions given in Fig. 2. The solid line corresponds to the fit from the Rietveld refinement. Bragg reflactions for *R3c* space group are indicated by sticks.

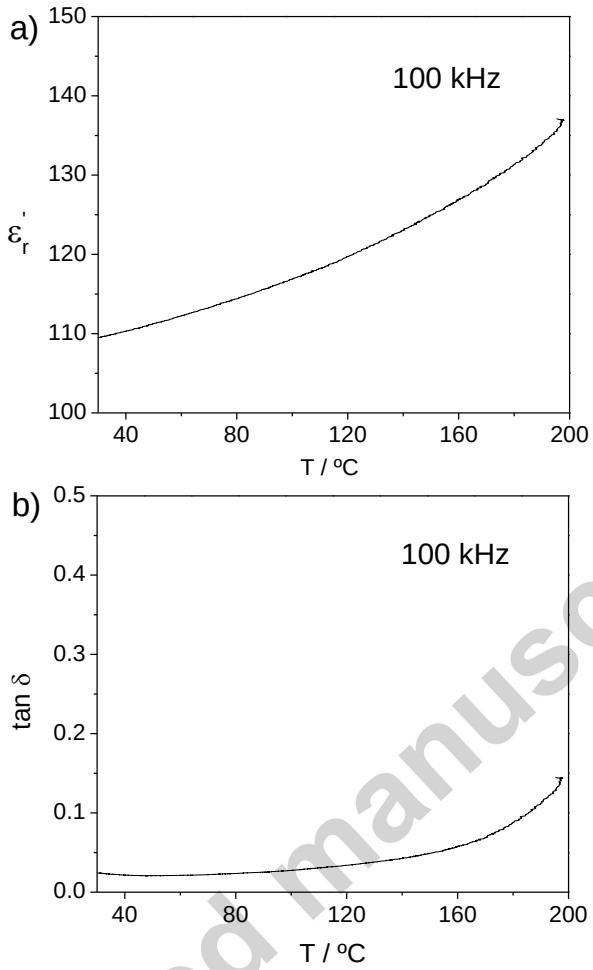


Figure 5. a) Relative permittivity ($\varepsilon_r$') and b) tan δ versus temperature for the $BiFeO_3$ pellet prepared by mechanosynthesis and flash sintered under the conditions given in Fig. 2.

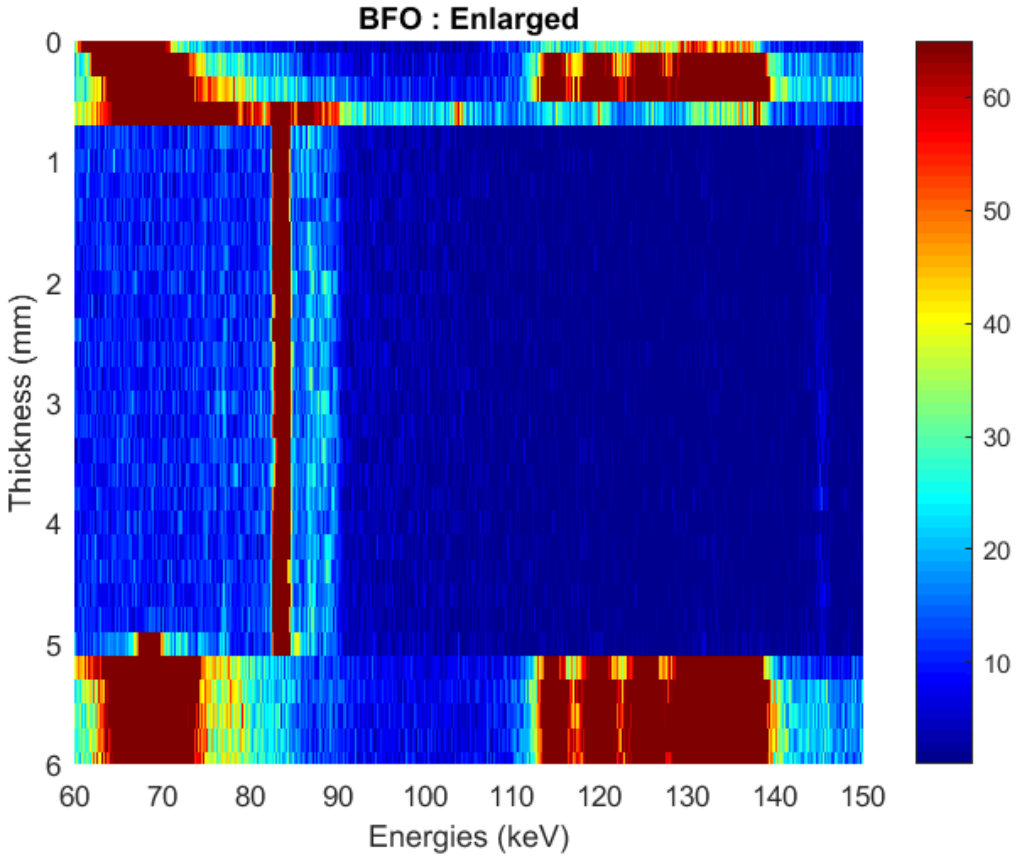


Figure 6. Diagram of a profile scan along the height of a $BiFeO_3$ sample pellet, during the stage III of a flash sintering experiment performed under the conditions given in Fig. 2.

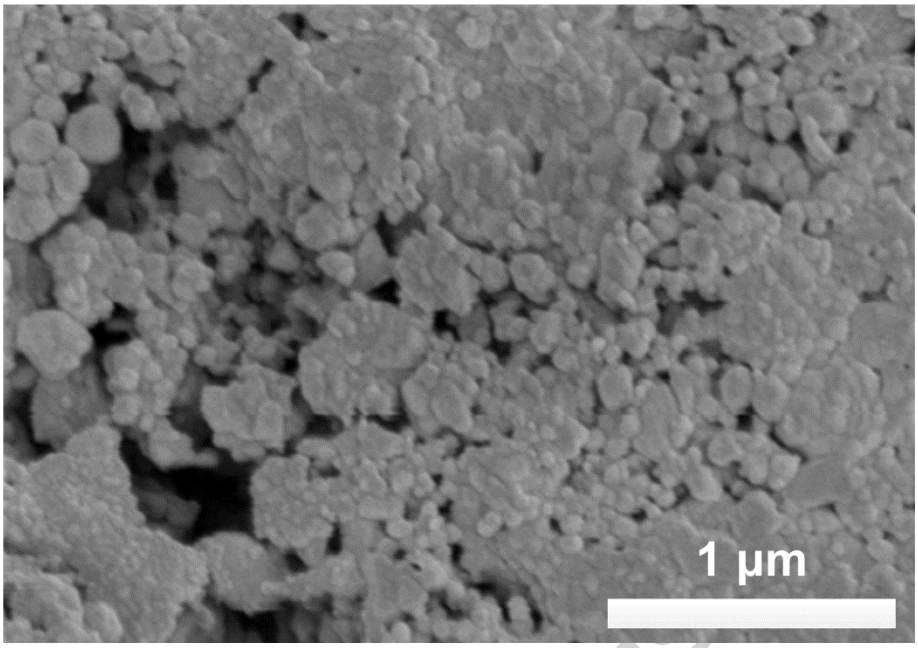


Figure 7. SEM micrograph of a cylindrical pellet (6 mm in diameter by 0.9 mm thickness) of $BiFeO_3$ rapidly sintered at 820 ºC for 75 seconds and quenched to room temperature.

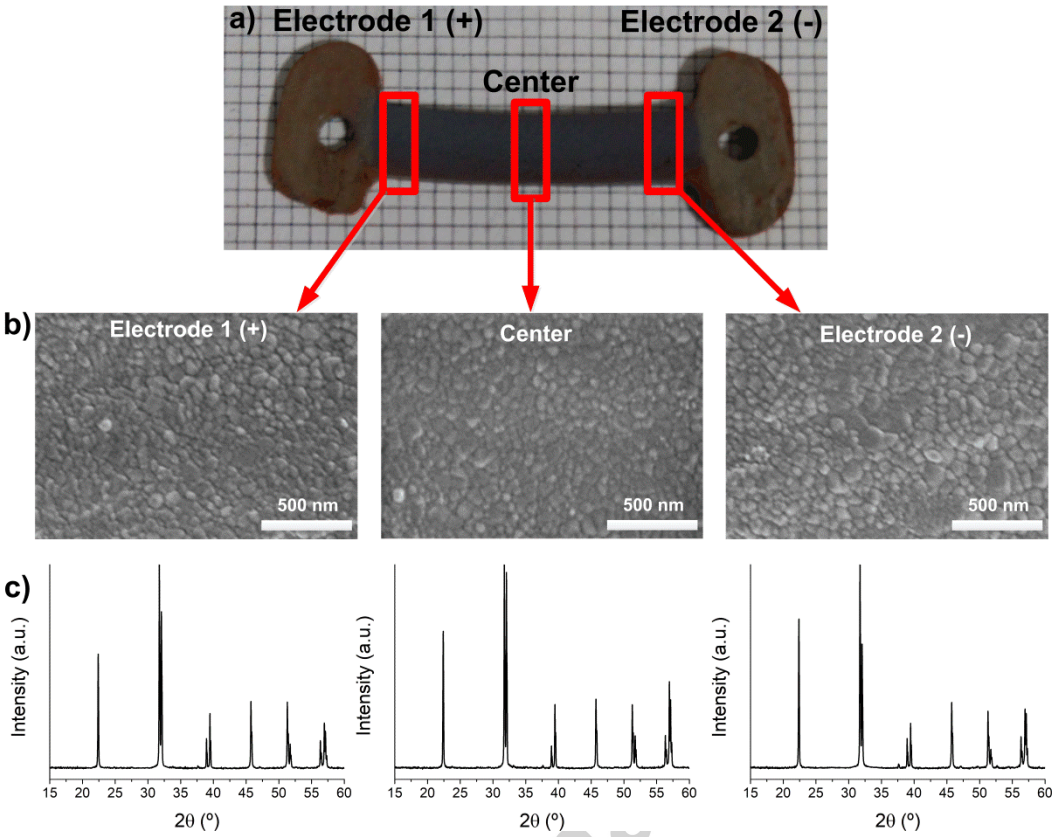


Figure 8. a) Dog-bone shaped sample of $BiFeO_3$ flash sintered at 60 V $cm^{-1}$ and 4 A $cm^{-2}$; b) SEM micrographs and c) XRD patterns of the different areas highlighted in a).